scientific reports

Check for updates

OPEN

# Thalamic oscillatory dysrhythmia and disrupted functional connectivity in thalamocortical loops in perinatal stroke

Anton Rogachov[1], Helen L. Carlson[2,3], Amanda Robertson[1,5], Trish Domi[5], Adam Kirton[2,3,4] & Nomazulu Dlamini[1,5]✉

**Periventricular venous infarction (PVI) is a subtype of perinatal stroke localized to subcortical white matter occurring before 34 weeks of gestation. An emerging body of literature has reported life-long motor impairments and compromised quality of life in patients with PVI. However, there remains a paucity of foundational knowledge regarding the underlying neurobiological mechanisms that underpin these outcomes. Recent studies (Ferradal et al. in Cereb Cortex 29:1218–1229, 2019) in brain imaging suggest that healthy development of thalamocortical connections is instrumental in coordinating brain connectivity in both prenatal and postnatal periods given the central role the thalamus and basal ganglia play in motor circuitry. Therefore, we provide a regional and cross-network approach to the analysis of interactive pathways of the thalamus, basal ganglia, and cortex to explore possible neurobiological disruptions responsible for clinical motor function in children with PVI. A resting-state fMRI protocol was administered to children with left periventricular venous infarction (PVI) (n = 23) and typically developing children (TDC) (n = 22) to characterize regional oscillatory and thalamocortical disturbances and compare them to clinical motor function. We hypothesized that PVI would affect resting-state measures of both regional and global brain function, marked by abnormally high amplitudes of regional oscillatory activity, as well as lower local and cross-network communication. Using a combination of robust functional metrics to assess spontaneous, oscillatory activity (Amplitude of Low-Frequency Fluctuations [ALFF] and fractional ALFF), as well as local (Regional Homogeneity [ReHo]) and cross-network connectivity (Degree Centrality [DC] and Functional Connectivity [FC]). We found that compared with TDC, children with PVI exhibited higher levels of ALFF, and these functional differences were associated with the severity of motor impairment. Moreover, the thalamus in children with PVI also showed lower connectivity in relaying thalamocortical pathways. These disruptions in thalamocortical pathways from the thalamus were localized to the medial prefrontal cortex (mPFC), a key hub of the default mode network). Collectively, our findings suggest that heightened levels of regional, oscillatory activity in the thalamus may disrupt more widespread thalamocortical cross-network circuity, possibly contributing to motor impairments in children with PVI.**

**Keywords** Perinatal stroke, Periventricular venous infarction, Venous stroke, Outcome, Imaging, Functional magnetic resonance imaging, Connectivity, Neural networks

Perinatal stroke refers to multiple types of focal brain lesions that occur due to a vascular injury in the brain between 20 weeks of gestation and the 28th postnatal day[1]. The incidence of perinatal stroke is greater than 1 in 1100 term newborns[2]. Perinatal stroke is the leading cause of hemiparetic cerebral palsy, leaving most survivors with variable degrees of lifelong motor disability[3–5]. Depending on the time of diagnosis and the vascular

[1]Division of Neurology, The Hospital for Sick Children, University of Toronto, 175 Elizabeth Street | 19th floor, Toronto, ON M5G 2G3, Canada. [2]Calgary Pediatric Stroke Program, Alberta Children's Hospital Research Institute, Calgary, AB, Canada. [3]Hotchkiss Brain Institute, University of Calgary, Calgary, AB, Canada. [4]Department of Pediatric and Clinical Neurosciences, Cumming School of Medicine, University of Calgary, Calgary, AB, Canada. [5]Neurosciences and Mental Health Department, The Hospital for Sick Children, Toronto, ON, Canada. ✉email: nomazulu.dlamini@sickkids.ca

lesion type, five subtypes of perinatal stroke are described: neonatal arterial ischemic stroke (NAIS), neonatal hemorrhagic stroke (NHS), neonatal cerebral sinovenous thrombosis (NCSVT), presumed perinatal arterial ischemic stroke (PPAIS), and periventricular venous infarction (PVI)[2].

Unlike the cortical and sub-cortical lesions of arterial ischemic stroke (AIS), which result from an occlusion of a cerebral artery, periventricular venous infarcts (PVI) are subcortical strokes which are isolated to the periventricular white matter (PVWM) in the medullary venous territory with distinct sparing of the cortex and basal ganglia and evidence of remote hemorrhage[4]. The presumed mechanism is regional venous infarction secondary to germinal matrix hemorrhage in the preterm fetus who is then born at term and presents later in infancy with hemiparesis[2,5–7].

Many neuroimaging studies have investigated neurological outcomes following perinatal AIS[8–11]. In contrast, despite a high prevalence and almost universal motor disability, the understanding of how PVI lesions contribute to morbidity remains poorly understood. Improved understanding of the neural mechanisms contributing to motor deficits in PVI is a necessary step to improve the increasingly well informed models of the developmental plasticity that occurs after perinatal stroke[12] to develop personalized rehabilitation strategies.

PVI lesions typically damage the descending corticospinal tracts and diffusion tractography studies support the simple concept that such direct motor pathway injury could explain contralateral hemiparesis[13,14]. However, more careful consideration suggests other functional networks may be altered. For example, studies indicate that within the DMN, a disruption in both intra- and inter-network connectivity correlate with motor impairments post-stroke)[15–17] and cognitive recovery[18–21]. Sensory pathways may also be disrupted by PVI lesions [22] though they are often able to "divert" their course to reach the sensory cortex[23]. PVI lesions do not typically cause direct structural damage to sub-cortical structures such as the basal ganglia and thalamus, though bilateral alterations in structures distant from injury such as the thalamus, also known as diaschisis, may occur in perinatal stroke[24].

The thalamus plays a central role in integrating and coordinating communication between diverse structures[25,26]. It is plausible that the differences in outcome seen in children with PVI may be related to the integrity of broader cerebral networks and the more widespread developmental alterations in neural circuitry that occur following such focal, perinatal injury. For example, the development of thalamocortical pathways during mid- to late gestational periods are instrumental in shaping the overall connectivity of the brain during prenatal and early postnatal stages of life[27–29]. Functional brain imaging studies have described the relationship between such thalamocortical connectivity and developmental outcomes[30]. A recent study of the entire white matter connectome in children with perinatal stroke found widespread alterations in structural connectivity throughout the contralesional hemisphere that were strongly associated with clinical motor outcomes[31]. A machine learning study combining diverse imaging biomarkers found that specific motor outcomes are best explained by considering numerous features in combination in children with perinatal stroke[32]. Such progress emphasizes the importance of considering diffuse brain networks connected to, or even entirely remote from, the site of injury in PVI to better understand neurological outcomes.

Resting-state BOLD fMRI provides a robust approach to investigate the relationship between brain function and clinical presentation. Specifically, the amplitude of regional BOLD low-frequency oscillations (LFO) and functional connectivity between brain regions and networks have been shown to be a meaningful marker of brain pathology across different clinical populations[33]. Here we used resting-state functional MRI to investigate cross-network and thalamocortical circuitry, and resulting associations with clinical motor function in children with PVI. Our hypotheses were that, compared with TDC, children with PVI will: (1) exhibit larger amplitude in the BOLD oscillations within the thalamus and basal ganglia, (2) demonstrate lower levels of local- and cross-network connectivity in regions showing abnormal oscillatory levels, and (3) show an association between the degree of functional aberrations (as captured by these metrics) and clinical motor function.

## Materials and methods

### Participants

Children with left-hemisphere PVI were recruited from three sites across Canada as a subset of a larger clinical trial (https://clinicaltrials.gov/ct2/show/NCT03216837). The three sites were located in Calgary and Edmonton (recruitment via the Alberta Perinatal Stroke Project), and Toronto (recruitment via the Hospital for Sick Kids and Holland-Bloorview Kids Rehabilitation Hospital)[34]. We included children with left-hemisphere PVI only to mitigate confounding laterality effects and to maintain appropriate uniformity for group-level analyses. Inclusion criteria were: (1) MRI-confirmed diagnosis of left-hemisphere PVI according to published criteria[6] as determined by a pediatric neurologist, (2) term birth (> 36 weeks gestation), (3) no history of other neurological disorders, unstable epilepsy, or multifocal or diffuse injuries, (4) age 6–19 years, (5) symptomatic unilateral cerebral palsy as described by a Manual Ability Classification System score of I-IV[35] and perceived disability by the child and family. For comparison, a cohort of right-handed, typically developing children (TDC) of similar age and sex with no neurological conditions or MRI contraindications were recruited from a Calgary-based healthy controls program. Parents or guardians provided informed written consent and written assent was given by patients. This study was approved by the local ethics boards at each of the recruiting sites (Universities of Calgary and Alberta [Edmonton], The Hospital for Sick Children, and Holland-Bloorview Kids Rehabilitation Hospital [Toronto]).

All research was performed in accordance with relevant guidelines/regulations. Informed consent was obtained from all participants and/or their legal guardians.

## Functional MRI

### Procedure and scanning

Patients were scanned with a Siemens 3 T Trim-Trio (Hospital for Sick Children, Toronto) or a GE 3 T 750W MRI scanner (Alberta Children's Hospital, Calgary). We acquired a high-resolution T1-weighted anatomical scan (3D IR-FSPGR sequence; 180 axial slices; repetition time (TR) = 1910 ms; echo time (TE) = 3.5 ms; flip angle = 11°; 256 × 256 matrix; 1 × 1 × 1 mm voxels) and a 5-min $T2^*$-weighted resting-state fMRI scan (gradient-echo imaging sequence; 36 transverse slices; TR = 2000 ms; TE = 30 ms; 64 × 64 matrix; 3.6 isotropic voxels; 150 volumes). Imaging data from the rest of patients was collected on a 3 T GE MR750w scanner with a 32-channel head coil. High-resolution T1-weighted anatomical images were obtained in an axial plane (FSPGR BRAVO; 166–225 slices; TR = 8.5 ms; TE = 3.2 ms; flip angle = 11°, 256 × 256 matrix; voxels = 1 × 1 × 1 mm) as well as a 5-min $T2^*$-weighted resting-state fMRI scan (voxels = 3.6 mm isotropic; 36 transverse slices, TR = 2000 ms; TE = 30 ms; flip angle = 90°; 150 volumes). During the resting-state sequence, patients were instructed to view a centrally presented fixation cross and think of "nothing in particular". Inter-site harmonization was addressed with a site visit at Sickkids, Toronto, where imaging staff from each team met with the MRI technician to ensure that the standardized MRI protocols were aligned between sites.

### Data preprocessing

Functional MRI data was preprocessed using an in-house pipeline using standard AFNI[36] and FSL[37] tools. Non-brain voxels were removed using AFNI's *3dSkullStrip* command and images were motion corrected by estimating spatial deviations between a reference functional image (the base image) and all other volumes using each of the six motion parameters. The deviation for each image was recorded in a 'motion' file, and used to censor volumes that contained excessive head motion. Timepoints with greater than 2 mm of maximum mean displacement were discarded, and patients with more than 1/3 of their volumes removed were excluded from analysis. Next, the functional images were registered to the skull-stripped, T1-weighted anatomical imaging using FLIRT (rigid-body transformation with 7 degrees of freedom), followed by nonlinear registration to MNI152_2mm space using FNIRT. Physiological noise was captured in the white matter (WM) and cerebrospinal fluid (CSF) via tissue segmentation using FSL's *fast* command, and nuisance signal from the WM, CSF, as well as head motion were regressed from the data.

*Overview of study analyses*

The primary goal of this study was to use a combination of functional metrics to quantify regional and cross-network activity. Towards this aim, we first quantified regional, frequency-specific alterations in amplitude of brain signal fluctuations, and examined associations with clinical motor function. Next, we examined how these regional functional alterations are implicated in larger, cross-network functional aberrations observed in patients. A summary of the functional metrics utilized is provided in Fig. 1.

*Regions of interest*

A region of interest (ROI) was used based on the Harvard–Oxford subcortical atlas (Fig. 2a) encompassing the bilateral thalamus and basal ganglia. ROIs from the bilateral thalamus, putamen, caudate nucleus, and globus pallidus were combined to construct a single mask. This mask was utilized to measure amplitude of low-frequency fluctuations (ALFF) (primary outcome), fractional ALFF (fALFF), regional homogeneity (ReHo), and degree centrality (DC). Furthermore, functional connectivity (FC) was measured between the sub-cortical ROI and cortical brain regions (Fig. 2b).

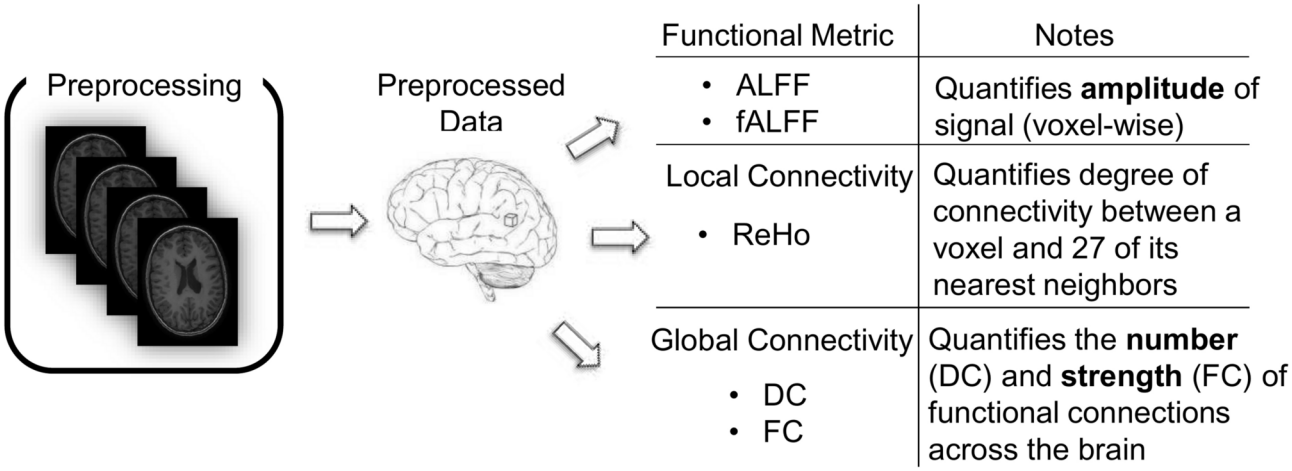


**Fig. 1**. Overview of functional metrics.

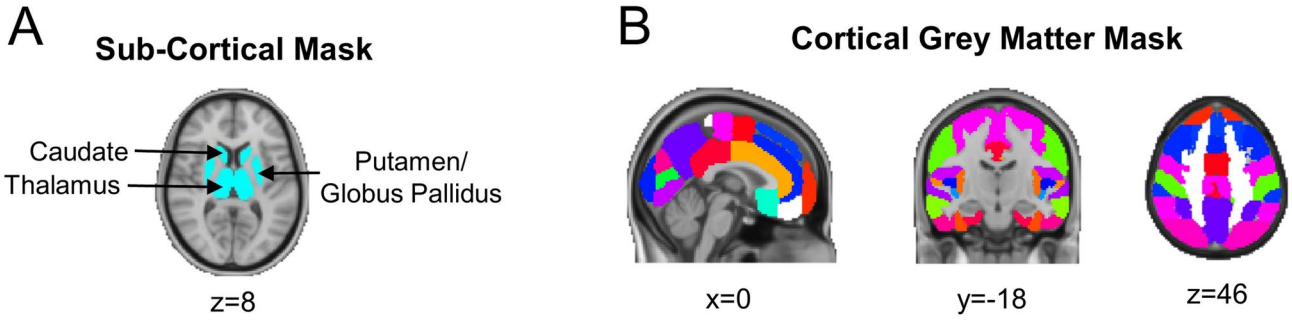


**Fig. 2**. Brain regions/masks of interest. (**A**) The sub-cortical mask was derived using the Harvard–Oxford Sub-Cortical atlas, and included the thalamus and basal ganglia (caudate, putamen, globus pallidus). (**B**) The cortical grey matter mask was derived using the Harvard–Oxford Cortical atlas and included all cortical, grey matter regions.

*Amplitude of low-frequency fluctuation analysis*

We investigated two Fast Fourier Transform (FFT)-based indices of BOLD amplitude: (1) ALFF[38], and (2) fALFF[39]. While ALFF has been suggested to reflect the energy/intensity of the oscillations, fALFF represents the relative contribution of oscillations within a specific frequency band to the whole detectable frequency. Both ALFF and fALFF have been reported to show high test–retest reliability, especially for measurements within grey matter, with reliability being greater in ALFF than fALFF[39].

After the functional data was spatially smoothed using a 6-mm radius full-width half-maximum (FWHM) Gaussian kernel, the SPM toolbox RESTV1.8[40] was used to temporally filter the BOLD signal time courses into three frequency bands (slow-wave 5: 0.01–0.027 Hz; slow-wave 4: 0.027–0.073 Hz; slow-wave 3: 0.073–0.198 Hz)[41] and calculate the amplitude maps on a voxel-wise basis for each subject. Furthermore, we divided ALFF values by the total power over the entire frequency range to obtain fractional ALFF (fALFF) brain maps for each subject.

*Local connectivity/regional homogeneity (ReHo)*

To investigate the relationship between regional oscillations and local network connectivity, we calculated Kendall's coefficient of concordance (KCC), which measures the functional synchronization of the time series of a given voxel and its nearest neighbors. This approach, known as Regional Homogeneity (ReHo), serves as the most efficient, reliable, and widely used index to calculate local FC[42]. ReHo describes the degree of connections between a given node and its nearest neighboring nodes, characterizing the importance of a node's local functional interactions in the human brain connectome[43]. Using the RESTV1.8 toolbox[40], the preprocessed, but not spatially smoothed, images were used to generate voxel-based ReHo values for each individual subject. For each voxel, the KCC was computed between its time course and the average time course of its 27 neighboring voxels.

*Degree centrality analysis*

DC calculations were performed to further assess how disruptions in regional oscillations relate to widespread communication throughout the brain. DC is among the most fundamental graph theory measures used to identify central, integrative hubs in the human brain[44,45]. These hubs are thought to be responsible for increasing the efficacy of brain function by coordinating information flow[46] and thus, minimizing metabolic demand by limiting the number of long-distance connections that integrate local network activity[47]. Using the RESTV1.8 toolbox[40], the preprocessed, temporal filtered (0.01–0.1 Hz) images were used to generate DC maps for each subject. Specifically, the connectivity between the time series extracted from a given voxel $i$ was computed with every other voxel within the cortical grey matter mask. Next, the correlation matrix was thresholded at a connectivity value of $r = 0.25$ to generate a binary, undirected matrix by setting all connectivity values below the threshold to 0 while the remaining ones were set to 1. The DC value for voxel $i$ was computed by taking the sum of all non-zero connections in this binary map.

*Functional connectivity analysis*

To build upon the DC results and to determine which areas of the cortex showed altered FC with the thalamus, we first masked the region that showed DC differences between PVI and TDC patients and extracted the BOLD signal time course from this region of interest for each patient. Then, FC was calculated via a Pearson's correlation between the extracted BOLD time courses and the BOLD time courses of every voxel in the cortical grey matter mask (Fig. 2b) using FSL's FEAT function. A Fisher $r$-to-$z$ transformation was performed to stabilize the variance of correlation values[48]. The first-level connectivity maps were then concatenated across all patients and were subject to non-parametric permutation testing using FSL's *Randomise* command[49].

*Analysis of voxel-wise functional metrics*

To compare ALFF, fALFF, ReHo, and DC values between patients with PVI and TDC, we first ran a 2-sample $t$-test between the two groups separately for each metric using *Randomise*, a non-parametric permutation tool in

FSL[50]. We masked the thalamus and basal ganglia regions and performed a voxel-wise permutation test (positive and negative contrasts; 5000 iterations) with Threshold-Free Cluster Enhancement (TFCE) for the ReHo and DC analyses as well as separately for each frequency band (slow-3, slow-4, and slow-5) for the ALFF and fALFF analyses. Although there were no differences in head motion on the group level ($p = 0.77$), head motion artifacts can still potentially alias into the BOLD signal[50] and remain a confound in our FC analysis[51,52]. Furthermore, the lesion volume within each patient was quantified using the recon-all -subcortseg command in FreeSurfer v7. A laterality index of lesion volume ((ipsilesional ventricular volume–contralesional ventricular volume) / ipsilesional ventricular volume + contralesional ventricular volume), as well as head motion, age, and sex were included as co-variates of no interest in the model. All presented results were thresholded at $p < 0.05$ (family-wise error [FWE] corrected for multiple comparisons).

*Clinical motor assessment*

Children with PVI completed a series of validated motor assessments administered by experienced pediatric occupational therapists who were blinded to all imaging features. The Assisting Hand Assessment (AHA) measures bilateral hand function in children with hemiplegic cerebral palsy. The AHA consists of 22 bimanual actions which evaluate the affected hand for general use, grasp and release, pace, coordination, and fine motor adjustment with performance quantified by a logit unit score[53]. Similarly, the Box and Block Test (BBT) assessed unilateral gross manual dexterity of both the affected (BBTA) and unaffected (BBTU) hands[54]. The raw score indicates the number of blocks that were moved from one box, over a physical barrier, and placed in another box within a 60 s period. Higher AHA, BBTA, and BBTU scores represent better performance.

*Regressing clinical scores against functional brain metrics*

Voxel-wise ALFF values from brain regions that showed significant differences in the group contrast between PVI and TDC were masked and regressed against BBTA, BBTU, and AHA scores separately using FSL's *Randomise* command. Age, sex, laterality index of lesion volume, and head motion were included in the model as co-variates of no interest. Non-parametric permutation testing (5000 iterations) using threshold-free cluster enhancement (TFCE) was used to determine statistical significance. All reported results were thresholded at $p < 0.05$, FWE-corrected for multiple comparisons.

## Results

### Patient population

Of the initial sample of 26 left-hemisphere PVI patients, one was excluded due to imaging registration issues, and two patients could not be age- and sex-matched, leaving the final analyses to be conducted on a cohort of twenty-three children with left PVI (13 males and 10 females; mean age ± SD: 11.9 y ± 2.5; range: 7.9–16.6 years old) and 22 TDC (12 males and 10 females; mean age ± SD: 12.7 y ± 2.8; range: 6.5–16.9 years old) with groups well matched for age and sex (age: $p = 0.31$; age: $p = 0.89$). Patient characteristics are reported in Table 1.

### PVI patients demonstrated elevated oscillatory activity in the ipsilesional thalamus

Children with PVI exhibited higher levels of ALFF consistently across the three frequency bands of interest compared with TDC. Within the slow-3, slow-4, and slow-5 frequency bands, patients with PVI exhibited elevated amplitudes of oscillatory activity confined to the ipsilesional thalamus (Fig. 3) (mean ± SEM ALFF values: slow-5 (Fig. 3a), PVI, 5.71 ± 0.30; TDC, 4.09 ± 0.25, *p-value* < 0.05, FWE-corrected; slow-4 (Fig. 3b), PVI, 6.12 ± 0.22, TDC, 4.74 ± 0.24, *p-value* < 0.05, FWE-corrected; slow-3 (Fig. 3c), PVI, 6.51 ± 0.20; TDC, 5.13 ± 0.26, *p-value* < 0.05, FWE-corrected). There were no brain regions in which ALFF was lower in stroke subjects as compared to TDC. Also, there were no group differences in fALFF in any region of our sub-cortical mask (Table 2).

### Reduced correlations from the thalamus to cortical grey matter in children with PVI

In order to assess more widespread brain networks, we first computed degree centrality to quantify the number of significant correlations between each voxel within our sub-cortical mask and all voxels in the cortical grey matter. The spatial distribution of the DC group differences followed a similar pattern as the oscillatory disruptions revealed with ALFF: the ipsilateral thalamus. The number of significant correlations was significantly lower in PVI patients within the ipsilesional thalamus (Fig. 4a) (mean ± SEM × $10^3$ degree centrality values: PVI, 17.8 ± 2.3; TDC, 24.9 ± 1.7, $p < 0.05$, FWE-corrected) but the same as controls from the contralateral thalamus.

### Altered FC between the thalamus and medial prefrontal cortex of the Default Mode Network

Voxels in the thalamus that demonstrated DC group differences were masked (Fig. 4a), their time series were averaged across the mask and extracted, and the strength of FC to the cortical grey matter was calculated. Compared with TDC, children with PVI had lower levels of FC between the thalamus and the mPFC (Fig. 4b) (mean ± SEM z-scored FC values: PVI, − 1.85 ± 0.37; TDC, 0.08 ± 0.23, $p < 0.05$, FWE-corrected).

### Thalamic oscillations are associated with clinical motor performance

Of the 23 patients with PVI, 17 completed the Box and Block Test. Higher slow-5 oscillatory amplitudes in the ipsilesional thalamus was associated with poorer motor performance of the affected hand (Fig. 5a) ($rho = -0.65$, $p < 0.05$) but not the unaffected hand (Fig. 5b) ($rho = -0.34$, $p > 0.05$). Slow-3 and Slow-4 oscillatory amplitudes showed no statistically significant relationships with BBT performance in either the affected or unaffected hand. Similarly, there was no significant relationship between AHA scores (n = 16) and oscillatory activity in the slow-3, slow-4, and slow-5 frequency bands.

| Patient ID | Age at scan | Sex | BBTA score | BBTU score | AHA score | Left ventricular volume ($mm^3$) | Right ventricular volume ($mm^3$) | Laterality index | Total intracranial volume ($mm^3$) |
|---|---|---|---|---|---|---|---|---|---|
| 01 | 13 | F | 24 | 32 | 83 | 16,771 | 9057 | 0.2987 | 1,713,675 |
| 02 | 13 | M | 40 | 56 | 62 | 13,700 | 5664 | 0.4150 | 1,525,678 |
| 03 | 10 | M | 34 | 44 | 74 | 3572 | 2868 | 0.1093 | 1,464,406 |
| 04 | 11 | M | 40 | 74 | 81 | 11,780 | 6608 | 0.2813 | 1,636,248 |
| 05 | 10 | F | 17 | 55 | 47 | 11,873 | 6917 | 0.2638 | 1,432,411 |
| 06 | 11 | F | 38 | 58 | 67 | 18,621 | 11,558 | 0.2315 | 1,670,353 |
| 07 | 10 | F | 27 | 41 | 67 | 5780 | 2307 | 0.4295 | 1,399,809 |
| 08 | 8 | M | 15 | 53 | 53 | 4913 | 6168 | −0.1132 | 1,543,930 |
| 09 | 14 | F | 30 | 60 | – | 35,767 | 15,217 | 0.4031 | 1,821,770 |
| 10 | 10 | F | 24 | 54 | 66 | 4381 | 2382 | 0.2956 | 1,550,926 |
| 11 | 17 | F | 26 | 63 | 59 | 7454 | 3053 | 0.4189 | 1,061,920 |
| 12 | 18 | M | 24 | 84 | 60 | 11,479 | 10,429 | 0.0479 | 1,804,380 |
| 13 | 15 | F | 40 | 67 | 65 | 3969 | 3765 | 0.0263 | 1,238,879 |
| 14 | 11 | M | 38 | 57 | 79 | 3122 | 1836 | 0.2594 | 1,234,758 |
| 15 | 13 | M | 50 | 63 | 86 | 3426 | 3302 | 0.0184 | 1,343,602 |
| 16 | 10 | M | 38 | 43 | 58 | 12,494 | 7557 | 0.2462 | 1,502,016 |
| 17 | 13 | M | 22 | 68 | 63 | 11,479 | 10,429 | 0.0479 | 1,718,421 |
| 18 | 11 | F | – | – | – | 5440 | 3459 | 0.2226 | 1,414,390 |
| 19 | 10 | M | – | – | – | 9662 | 4409 | 0.3733 | 1,569,843 |
| 20 | 12 | F | – | – | – | 11,394 | 5906 | 0.3172 | 1,509,430 |
| 21 | 11 | M | – | – | – | 5974 | 4608 | 0.1291 | 1,532,492 |
| 22 | 16 | M | – | – | – | 13,021 | 9421 | 0.1604 | 1,592,912 |
| 23 | 9 | M | – | – | – | 13,522 | 3416 | 0.5967 | 1,416,146 |

**Table 1**. Patient demographics.

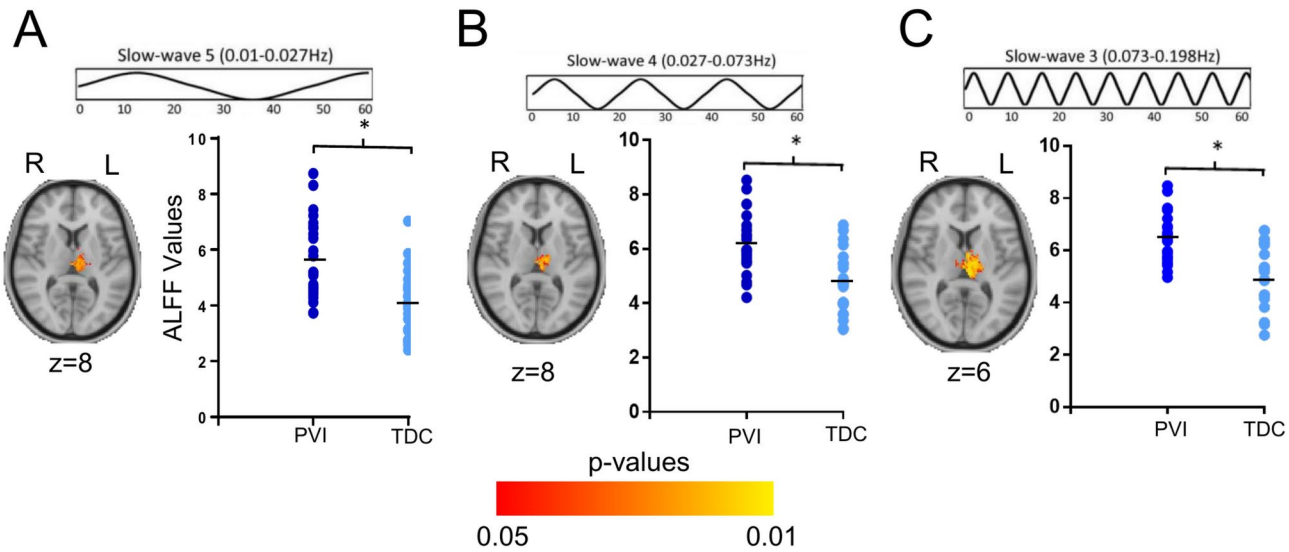


**Fig. 3**. Frequency-specific group differences in ALFF. The contrast maps represent the differences in ALFF between children with PVI ($n = 23$) and TDC ($n = 22$) within three frequency bands: slow-5 (0.01–0.027 Hz), slow-4 (0.027–0.073 Hz), and slow-3 (0.073–0.198 Hz). The dot plots represent individuals' ALFF values averaged across the significant cluster. All statistical images display significant clusters at $p < 0.05$, FWE-corrected. All axial brain slices are represented in radiological orientation.

## Discussion

Our study used resting-state fMRI to characterize fluctuations of BOLD signal in the basal ganglia and thalamus as well as thalamocortical connectivity in children with PVI. This study demonstrates that, compared with typically developing children, patients who incurred a PVI exhibited higher oscillatory amplitudes at rest in the

| Functional metric | Brain region | Peak location (x,y,z) | Cluster size (Voxels) | Frequency band |
|---|---|---|---|---|
| Amplitude (ALFF) | Thalamus | 2, − 16, 2 | 317 | Slow-wave 5 (0.01–0.027 Hz) |
| Amplitude (ALFF) | Thalamus | 0, − 20, 6 | 279 | Slow-wave 4 (0.027–0.073 Hz) |
| Amplitude (ALFF) | Thalamus | − 6, − 26, 8 | 720 | Slow-wave 3 (0.073–0.198 Hz) |
| Local connectivity (ReHo) | – | – | – | – |
| Number of significant connections (DC) | Thalamus | − 8, − 6, 12 | 124 | 0.01–0.1 Hz |
| DC number of significant connections (DC) | Thalamus | 12, − 16, 12 | 14 | 0.01–0.1 Hz |
| Functional connectivity (FC) | mPFC | − 6, 44, − 14 | 10 | 0.01 Hz-0.1 Hz |

**Table 2**. Summary of Results.

ipsilesional thalamus, an effect that was associated with the severity of clinical motor impairment. Furthermore, the ipsilesional thalamus demonstrated disrupted connectivity within the mPFC of the default mode network. These results suggest that regional thalamic dysrhythmia may contribute to the breakdown of more widespread, cross-network connectivity across the brain, highlighting a plausible mechanism underlying patients' clinical symptoms and outcome.

There is a growing body of literature reporting how regional BOLD oscillatory activity is associated with individual differences in psychophysical metrics in healthy individuals[55], severity of patients' symptoms across different disorders, including chronic pain[56,57], medial temporal lobe epilepsy[58], and bipolar disorder[59], as well as successful therapeutic intervention in chronic pain patients[60]. Our findings of higher levels of thalamic oscillatory amplitudes in PVI patients compared to typically developing peers is consistent with these studies and could arise through several mechanisms. For example, Craig and colleagues[24] (2019) reported smaller ipsilesional thalamic volume in children with perinatal stroke. Smaller thalamic volumes may suggest the presence of fewer thalamic neurons resulting in a compensatory heightened neuronal activity at rest, reflected by elevated oscillatory BOLD activity. Importantly, slow-5 oscillatory disruptions within the dorsomedial thalamus was associated with the degree of motor impairment in the affected hand only, and not in the unaffected hand, demonstrating functional specificity. While the neurobiological relevance of frequency-specific BOLD oscillations remains to be elucidated, tracing studies in non-human primates have shown that the dorsomedial thalami form reciprocal connections with multiple cortical areas, such as the prefrontal cortex and supplementary motor area, which are involved in integrating sensory and motor information, as well as coordinating sequences of action[61]. Moreover, the dorsomedial thalamus also receives inputs from subcortical structures, including the basal ganglia, and therefore serves as a key node for frontal-striatal-thalamic neural circuits and subsequent integrations of motoric information within the prefrontal cortexx[62]. As such, functional impairments that originate in the thalamus may play a key role in dictating and maintaining disruptions in broader neural circuitry underlying patients' motor deficits.

One such effect is thalamic diaschisis, or the alteration in brain structures remote but connected to the stroke lesion, which has been detailed in perinatal stroke[24]. Establishing the role of diaschisis in global connectivity changes may reveal the direct consequence of a local lesion on brain network organization, and may help guide mechanism-based neuromodulation treatment strategies. Similar to the localization of oscillatory differences, the ipsilateral thalamus also exhibited lower degree centrality in patients, suggesting different neuronal signaling and communication compared to TDC. The consistency of functional impairments across different metrics posits the thalamus as a key orchestrator of connectivity disruptions in which changes in coupling with remote networks may be due to lost afferents in this functionally lesioned hub of the network[63]. Moreover, network analysis in connectomics suggest that functional hubs play an integral role in global brain communication[46,64,65], with disturbances of hub regions causing severe impairments to their global integrative processes[66] and subsequent pathological manifestations of brain dysfunction[67]. In particular, we localized the cross-network disturbance to communication between the thalamus and the mPFC, two core hubs of the default mode network (DMN). It has been well-established that activity of the default mode and sensorimotor networks are anti-correlated in controls. It is plausible the initial disturbance in the sensorimotor network in patients with PVI may have affected the anti-correlations with the DMN. The mPFC is implicated in a variety of cognitive and executive functions, such as working memory, inhibitory control, and decision making[68]. This disruption in thalamocortical connectivity may underlie cognitive disability in children with PVI[69]. Connectivity measures within the reported thalamocortical circuitry may serve as a novel therapeutic target[70–72] for non-invasive brain stimulation therapies which have recently shown promising results in this population[10].

Several considerations are also pertinent to this study. It should be noted that head motion was pervasive in our cohort, and is known to have spurious but systematic effects on functional connectivity[51]. However, the fact that patients with excessive head motion were excluded, residual head motion was included as a co-variate of no interest in all of our statistical models, and there were no differences in head motion on a group level reduces the possibility that the reported group effects are driven by head motion. Also, after restricting our analysis to children with only left-hemisphere PVI and excluding patients due to other technical considerations the resulting sample size was modest. Despite these challenges, we believe this work provides an informative assessment of the functional impairments associated with PVI in perinatal stroke and establishes fundamental groundwork that should be investigated prior to and following intervention to better understand the neuroplasticity and re-organization that occurs with successful treatment outcomes.

In summary, we provide evidence highlighting the importance of the thalamus in sub-serving thalamocortical connectivity differences that are associated with motor impairments in children with periventricular venous infarction. While future studies may elaborate more on how these disruptions change following successful treatment outcome, this work reveals the importance of foundational neural circuitry implicated in PVI. These mechanistic underpinnings may guide future interventional strategies to restore specific thalamocortical circuits to alleviate clinical symptoms.

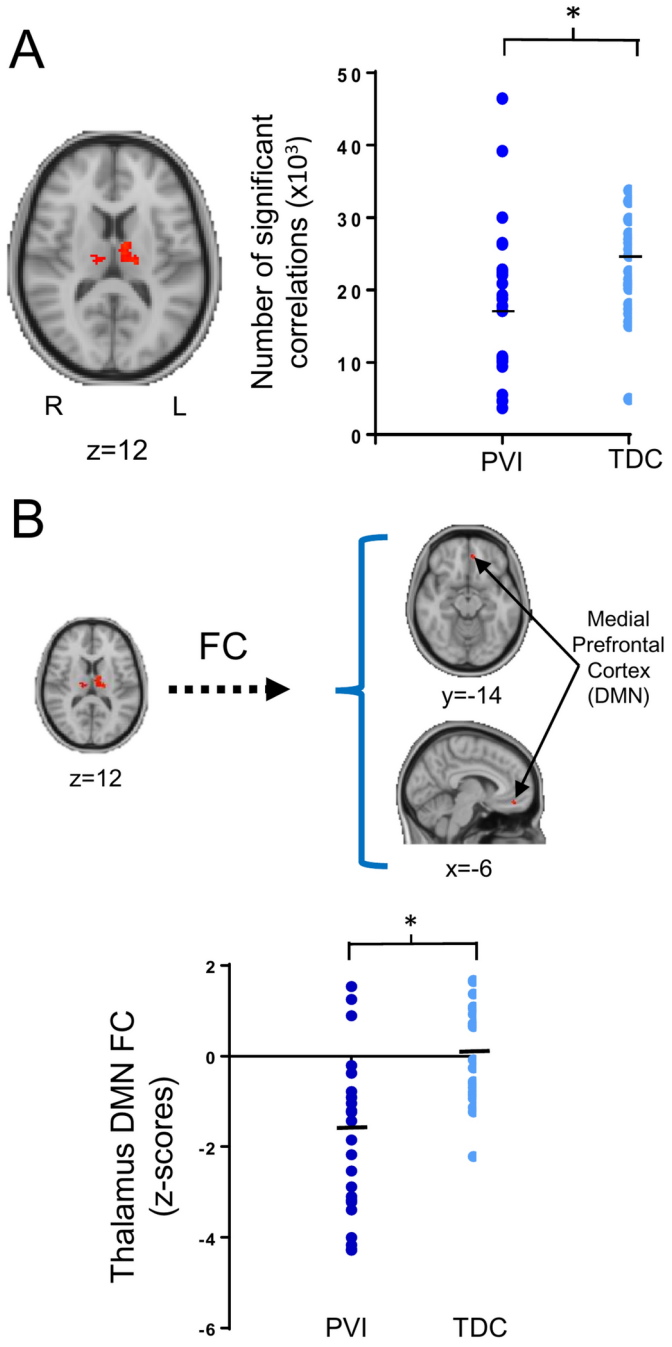


**Fig. 4**. Group differences in cross-network connectivity. (**A**) The contrast brain map represents brain regions that show group differences in the number of significant connections (DC) between the sub-cortical and cortical grey matter masks. The dot plot represents the number of significant connections between the marked brain regions (thalamus) and the cortex for every individual. (**B**) The contrast maps illustrate thalamocortical loops that show functional connectivity group differences. The dot plot in the lower half of the panel represent the r-to-z transformed FC values between the thalamus and mPFC for each subject. All statistically images display significant clusters at $p < 0.05$, FWE-corrected. All axial brain slices are represented in radiological orientation.

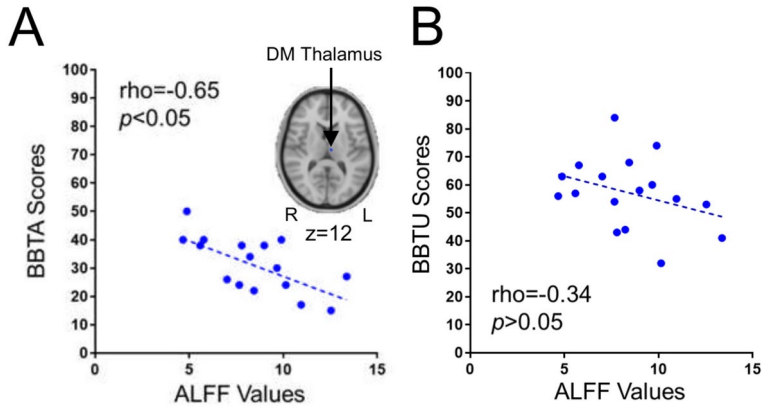


**Fig. 5**. Thalamic oscillations relate to unilateral hand motor performance. (**A**) Negative, significant correlation between BBT scores of the affected hand and ALFF values from the dorsomedial thalamus ($rho = -0.65$, $p < 0.05$, $n = 17$). The axial brain slice is shown in radiological orientation. (**B**) No statistically significant relationship between BBT scores of the unaffected hand and ALFF values from the dorsomedial thalamus ($rho = -0.34$, $p > 0.05$, $n = 17$).

## Data availability

The datasets used and/or analysed during the current study is available from the corresponding author on reasonable request.

Received: 30 July 2024; Accepted: 21 March 2025
Published online: 12 April 2025

## References

1. Ferradal, S. L. et al. System-specific patterns of thalamocortical connectivity in early brain development as revealed by structural and functional MRI. *Cereb. Cortex* **29**, 1218–1229 (2019).
2. Dunbar, M. & Kirton, A. Perinatal stroke: Mechanisms, management, and outcomes of early cerebrovascular brain injury. *Lancet Child Adolesc. Health* **2**, 666–676 (2018).
3. Dunbar, M. et al. Population based birth prevalence of disease-specific perinatal stroke. *Pediatrics* **146**, 11 (2020).
4. Kirton, A. et al. Presumed perinatal ischemic stroke: vascular classification predicts outcomes. *Ann. Neurol.* **63**, 436–443 (2008).
5. Takanashi, J. et al. Magnetic resonance imaging confirms periventricular venous infarction in a term-born child with congenital hemiplegia. *Dev. Med. Child Neurol.* **47**, 706–708 (2005).
6. Kirton, A. & Wei, X. Teaching neuroimages: Confirmation of prenatal periventricular venous infarction with susceptibility-weighted MRI. *Neurology* **74**, e48 (2010).
7. Kirton, A. et al. Risk factors and presentations of periventricular venous infarction vs arterial presumed perinatal ischemic stroke. *Arch. Neurol.* **67**, 842–848 (2010).
8. Boardman, J. P. et al. Magnetic resonance image correlates of hemiparesis after neonatal and childhood middle cerebral artery stroke. *Pediatrics* **115**, 321–326 (2005).
9. Dlamini, N. et al. Arterial wall imaging in pediatric stroke. *Stroke* **49**, 891–898 (2018).
10. Kirton, A. et al. Diffusion imaging of cerebral diaschisis in childhood arterial ischemic stroke. *Int. J. Stroke* **11**, 1028–1035 (2016).
11. Srivastava, R. et al. Diffusion imaging of cerebral diaschisis in neonatal arterial ischemic stroke. *Pediatr. Neurol.* **100**, 49–54 (2019).
12. Kirton, A. et al. Perinatal stroke: Mapping and modulating developmental plasticity. *Nat. Rev. Neurol.* **17**, 415–432 (2021).
13. Hodge, J. et al. segmental diffusion properties of the corticospinal tract and motor outcome in hemiparetic children with perinatal stroke. *J. Child Neurol.* **32**, 550–559 (2017).
14. Kuczynski, A. M. et al. Corticospinal tract diffusion properties and robotic visually guided reaching in children with hemiparetic cerebral palsy. *Hum. Brain Mapp.* **39**, 1130–1144 (2018).
15. Li, Y. et al. Aberrant interhemispheric functional reciprocities of the default mode network and motor network in subcortical ischemic stroke patients with motor impairment: A longitudinal study. *Front. Neurol.* **13**, 996621 (2022).
16. Wu, C. W. et al. Synchrony between default-mode and sensorimotor networks facilitates motor function in stroke rehabilitation: A pilot fMRI study. *Front. Neurosci.* **14**, 548 (2020).
17. Zhao, Z. et al. Altered intra- and inter-network functional coupling of resting-state networks associated with motor dysfunction in stroke. *Hum. Brain Mapp.* **39**, 3388–3397 (2018).
18. Vicentini, J. E. et al. Subacute functional connectivity correlates with cognitive recovery six months after stroke. *Neuroimage Clin.* **29**, 102538 (2021).
19. Tuladhar, A. M. et al. Default mode network connectivity in stroke patients. *PLoS ONE* **8**, e66556 (2013).
20. Park, J.-Y. et al. Significance of longitudinal changes in the default-mode network for cognitive recovery after stroke. *Eur. J. Neurosci.* **40**, 2715–2722 (2014).
21. Dacosta-Aguayo, R. et al. Impairment of functional integration of the default mode network correlates with cognitive outcome at three months after stroke. *Hum. Brain Mapp.* **36**, 577–590 (2015).
22. Kuczynski, A. M. et al. Sensory tractography and robot-quantified proprioception in hemiparetic children with perinatal stroke. *Hum. Brain Mapp.* **38**, 2424–2440 (2017).
23. Staudt, M. (Re-)organization of the developing human brain following periventricular white matter lesions. *Neurosci. Biobehav. Rev.* **31**, 1150–1156 (2007).
24. Craig, B. T., Carlson, H. L. & Kirton, A. Thalamic diaschisis following perinatal stroke is associated with clinical disability. *Neuroimage Clin.* **21**, 101660 (2019).
25. Haber, S. & McFarland, N. R. The place of the thalamus in frontal cortical-basal ganglia circuits. *Neuroscientist* **7**, 315–324 (2001).

26. Haber, S. N. & Calzavara, R. The cortico-basal ganglia integrative network: the role of the thalamus. *Brain Res. Bull.* **78**, 69–74 (2009).
27. Kostović, I. & Judas, M. The development of the subplate and thalamocortical connections in the human foetal brain. *Acta Paediatr.* **99**, 1119–1127 (2010).
28. McQuillen, P. S. & Ferriero, D. M. Perinatal subplate neuron injury: Implications for cortical development and plasticity. *Brain Pathol.* **15**, 250–260 (2005).
29. Ghosh, A. et al. Requirement for subplate neurons in the formation of thalamocortical connections. *Nature* **347**, 179–181 (1990).
30. Ball, G. et al. The influence of preterm birth on the developing thalamocortical connectome. *Cortex* **49**, 1711–1721 (2013).
31. Craig, B. T. et al. Developmental neuroplasticity of the white matter connectome in children with perinatal stroke. *Neurology* **95**, e2476–e2486 (2020).
32. Carlson, H. L. et al. Structural and functional connectivity of motor circuits after perinatal stroke: A machine learning study. *Neuroimage Clin.* **28**, 102508 (2020).
33. Fox, M. D. & Raichle, M. E. Spontaneous fluctuations in brain activity observed with functional magnetic resonance imaging. *Nat. Rev. Neurosci.* **8**, 700–711 (2007).
34. Cole, L. et al. Clinical characteristics, risk factors, and outcomes associated with neonatal hemorrhagic stroke: A population-based case-control study. *JAMA Pediatr.* **171**, 230–238 (2017).
35. Eliasson, A.-C. et al. The Manual Ability Classification System (MACS) for children with cerebral palsy: Scale development and evidence of validity and reliability. *Dev. Med. Child Neurol.* **48**, 549–554 (2006).
36. Cox, R. W. AFNI: Software for analysis and visualization of functional magnetic resonance neuroimages. *Comput. Biomed. Res.* **29**, 162–173 (1996).
37. Jenkinson, M. et al. FSL. *Neuroimage* **62**, 782–790 (2012).
38. Zang, Y.-F. et al. Altered baseline brain activity in children with ADHD revealed by resting-state functional MRI. *Brain Dev.* **29**, 83–91 (2007).
39. Zou, Q.-H. et al. An improved approach to detection of amplitude of low-frequency fluctuation (ALFF) for resting-state fMRI: Fractional ALFF. *J. Neurosci. Methods* **172**, 137–141 (2008).
40. Song, X.-W. et al. REST: A toolkit for resting-state functional magnetic resonance imaging data processing. *PLoS ONE* **6**, e25031 (2011).
41. Buzsáki, G. & Draguhn, A. Neuronal oscillations in cortical networks. *Science* **304**, 1926–1929 (2004).
42. Zuo, X.-N. et al. Toward reliable characterization of functional homogeneity in the human brain: preprocessing, scan duration, imaging resolution and computational space. *Neuroimage* **65**, 374–386 (2013).
43. Jiang, L. & Zuo, X.-N. Regional homogeneity: A multimodal, multiscale neuroimaging marker of the human connectome. *Neuroscientist* **22**, 486–505 (2016).
44. Buckner, R. L. et al. Cortical hubs revealed by intrinsic functional connectivity: mapping, assessment of stability, and relation to Alzheimer's disease. *J. Neurosci.* **29**, 1860–1873 (2009).
45. Cole, M. W., Pathak, S. & Schneider, W. Identifying the brain's most globally connected regions. *Neuroimage* **49**, 3132–3148 (2010).
46. Sporns, O., Honey, C. J. & Kötter, R. Identification and classification of hubs in brain networks. *PLoS ONE* **2**, e1049 (2007).
47. Bassett, D. S. & Bullmore, E. Small-world brain networks. *Neuroscientist* **12**, 512–523 (2006).
48. Thompson, W. H. & Fransson, P. On stabilizing the variance of dynamic functional brain connectivity time series. *Brain Connect* **6**, 735–746 (2016).
49. Winkler, A. M. et al. Permutation inference for the general linear model. *Neuroimage* **92**, 381–397 (2014).
50. Cordes, D. et al. Frequencies contributing to functional connectivity in the cerebral cortex in "resting-state" data. *AJNR Am. J. Neuroradiol.* **22**, 1326–1333 (2001).
51. Power, J. D. et al. Spurious but systematic correlations in functional connectivity MRI networks arise from subject motion. *Neuroimage* **59**, 2142–2154 (2012).
52. Van Dijk, K. R. A., Sabuncu, M. R. & Buckner, R. L. The influence of head motion on intrinsic functional connectivity MRI. *Neuroimage* **59**, 431–438 (2012).
53. Krumlinde-Sundholm, L. et al. The Assisting Hand Assessment: Current evidence of validity, reliability, and responsiveness to change. *Dev. Med. Child Neurol.* **49**, 259–264 (2007).
54. Mathiowetz, V. et al. Adult norms for the Box and Block Test of manual dexterity. *Am. J. Occup. Ther.* **39**, 386–391 (1985).
55. Rogachov, A. et al. Regional brain signal variability: A novel indicator of pain sensitivity and coping. *Pain* **157**, 2483–2492 (2016).
56. Alshelh, Z. et al. Chronic neuropathic pain: It's about the rhythm. *J. Neurosci.* **36**, 1008–1018 (2016).
57. Rogachov, A. et al. Abnormal low-frequency oscillations reflect trait-like pain ratings in chronic pain patients revealed through a machine learning approach. *J. Neurosci.* **38**, 7293–7302 (2018).
58. Protzner, A. B. et al. Characterizing functional integrity: Intraindividual brain signal variability predicts memory performance in patients with medial temporal lobe epilepsy. *J. Neurosci.* **33**, 9855–9865 (2013).
59. Martino, M. et al. Contrasting variability patterns in the default mode and sensorimotor networks balance in bipolar depression and mania. *Proc. Natl. Acad. Sci. U S A* **113**, 4824–4829 (2016).
60. Rogachov, A. et al. Plasticity in the dynamic pain connectome associated with ketamine-induced neuropathic pain relief. *Pain* **160**, 1670–1679 (2019).
61. McFarland, N. R. & Haber, S. N. Thalamic relay nuclei of the basal ganglia form both reciprocal and nonreciprocal cortical connections, linking multiple frontal cortical areas. *J. Neurosci.* **22**, 8117–8132 (2002).
62. Mitchell, A. S. & Chakraborty, S. What does the mediodorsal thalamus do?. *Front. Syst. Neurosci.* **7**, 37 (2013).
63. Campo, P. et al. Remote effects of hippocampal sclerosis on effective connectivity during working memory encoding: A case of connectional diaschisis?. *Cereb. Cortex* **22**, 1225–1236 (2012).
64. van den Heuvel, M. P. & Sporns, O. Network hubs in the human brain. *Trends Cogn. Sci.* **17**, 683–696 (2013).
65. de Reus, M. A. & van den Heuvel, M. P. Rich club organization and intermodule communication in the cat connectome. *J. Neurosci.* **33**, 12929–12939 (2013).
66. van den Heuvel, M. P. et al. Abnormal rich club organization and functional brain dynamics in schizophrenia. *JAMA Psychiat.* **70**, 783–792 (2013).
67. Bullmore, E. & Sporns, O. The economy of brain network organization. *Nat. Rev. Neurosci.* **13**, 336–349 (2012).
68. Livingston-Thomas, J. M. et al. Assessing cognitive function following medial prefrontal stroke in the rat. *Behav. Brain Res.* **294**, 102–110 (2015).
69. Lõo, S. et al. Long-term neurodevelopmental outcome after perinatal arterial ischemic stroke and periventricular venous infarction. *Eur. J. Paediatr. Neurol.* **22**, 1006–1015 (2018).
70. Grefkes, C. et al. Modulating cortical connectivity in stroke patients by rTMS assessed with fMRI and dynamic causal modeling. *Neuroimage* **50**, 233–242 (2010).
71. Grefkes, C. & Fink, G. R. Disruption of motor network connectivity post-stroke and its noninvasive neuromodulation. *Curr. Opin. Neurol.* **25**, 670–675 (2012).
72. Rehme, A. K. & Grefkes, C. Cerebral network disorders after stroke: Evidence from imaging-based connectivity analyses of active and resting brain states in humans. *J. Physiol.* **591**, 17–31 (2013).

## Acknowledgements
The authors thank the children and families for their generous participation in this study, Marlee Vandewouw for the development of the preprocessing pipeline/scripts, and the Auxillium Foundation for its generous support.

## Author contributions
A.R. wrote the main manuscript text and prepared figures. All authors reviewed the manuscript.

## Funding
This study was funded by the Canadian Institutes of Health Research (CIHR), the Heart and Stroke Foundation of Canada, the Auxillium Foundation, and the Restracomp Fellowship Award.

## Competing interests
The authors declare no competing interests.

## Additional information
**Correspondence** and requests for materials should be addressed to N.D.

**Reprints and permissions information** is available at www.nature.com/reprints.

**Publisher's note** Springer Nature remains neutral with regard to jurisdictional claims in published maps and institutional affiliations.